

1 A Climatology of UV Radiation, 1979–2000, 65S–65N

Julia Lee-Taylor¹, Sasha Madronich¹, Christopher Fischer¹,
and Bernhard Mayer²

¹ National Center for Atmospheric Research, Boulder, Colorado, USA

² Deutsches Zentrum für Luft- und Raumfahrt, Oberpfaffenhofen, Germany

Abstract Solar ultraviolet (UV) radiation reaching earth's surface is of interest because of its role in the induction of various biological and chemical processes, including skin cancer. We present climatological distributions of monthly mean surface-level UV radiation, calculated using the Tropospheric Ultraviolet-Visible (TUV) radiative transfer model with inputs of ozone column amounts and cloud reflectivities (at 380 nm) measured by satellite instruments (Total Ozone Mapping Spectrometers (TOMS), aboard Nimbus-7, Meteor-3, and Earth Probe). The climatology is averaged over the years 1979–2000 for UV-A (315 nm–400 nm), UV-B (280 nm–315 nm), and radiation weighted by the action spectra for the induction of erythema (skin-reddening), pre-vitamin D₃ synthesis, and non-melanoma carcinogenesis. Coverage is global, excluding the poles.

Comparisons with concurrent ground-based UV radiation measurements archived at the World Ozone and Ultraviolet Data Center show agreement at the 10%–20% level, except at high latitudes where the large surface albedo of snow and ice invalidates the use of satellite-observed reflectivity in estimating cloud cover. The climatology may be useful in epidemiological studies that assess the role of long-term environmental exposure to UV radiation.

Keywords UV climatology, erythema, vitamin D synthesis, TUV model

1.1 Introduction

Solar ultraviolet radiation transmitted through the atmosphere to earth's surface is known to induce various biological and chemical processes, many of which are harmful to living tissues and some materials (see UNEP, 2006, for a review). Examples of processes relevant to human health include skin-reddening (erythema), synthesis of vitamin D within skin, and induction of various skin cancers. The

long-term geographical distribution of surface UV radiation is of considerable interest towards understanding these effects. However, environmental UV levels are highly variable due to daily and seasonal cycles at different latitudes, and to variations in atmospheric transmission (mainly attributable to variations in ozone, clouds, and aerosols) and surface reflections. Ultraviolet radiation measurements by ground-based instruments are too few, and their record relatively short, to construct a unified picture of its average global distribution.

An alternative method of estimating surface UV levels with long-term global coverage relies on satellite-based observations of earth's atmosphere and surface, combined with a computer model of the propagation of UV radiation through the atmosphere. This methodology is already in use on a NASA website (http://jwocky.gsfc.nasa.gov/ery_uv/ery_uv1.html, which uses data from the TOMS ozone-monitoring satellite instruments to generate maps of erythematous UV for specific days. Other applications of the technique have illuminated interesting aspects of the problem, i.e., estimation of zonal mean irradiances at different UV wavelengths, of trends due to ozone changes, of cloud effects, and of geographical distributions based on monthly averaged ozone and clouds (e.g., Frederick and Lubin, 1988; Madronich, 1992; Eck et al., 1995; Frederick and Erlick, 1995; Herman et al., 1996a; Lubin et al., 1998; Herman et al., 1999; Sabziparvar et al., 1999; Herman et al., 2000; McKenzie et al., 2001). Here we use satellite-based observations of atmospheric ozone and clouds to derive a climatology of erythematous UV radiation with nearly global coverage (excluding the polar regions), averaged over the years 1979–2000. We developed a fast method for the explicit calculation of UV daily doses for each day of the whole time period. Averaging daily UV doses, rather than calculating monthly doses on the bases of monthly-averaged cloudiness and ozone, reduces possible uncertainties connected with the non-linear relationship between atmospheric parameters (e.g., total ozone and clouds) and surface UV radiation. Comparisons with long-term measurements at 22 UV monitoring stations allow some assessment of the reliability of this technique. Climatologies such as those presented here can be useful in epidemiological studies that assess the role of long-term environmental exposure to ultraviolet radiation, such as those discussed in Chapter 2 (McKenzie and Liley).

1.2 Method

UV broadband irradiances (W m^{-2}) are computed as integrals over wavelength λ (nm) of spectral irradiances $E(\lambda)$ ($\text{W m}^{-2} \text{nm}^{-1}$) weighted by appropriate spectral functions $S(\lambda)$ (typically unit-less):

$$\text{Irradiance} = \int S(\lambda) E(\lambda) d\lambda$$

$E(\lambda)$ is a function of solar zenith angle (SZA) and surface elevation, as well as

optical depth profiles of atmospheric absorbers and scatterers (e.g., ozone and clouds). The values of $S(\lambda)$ are unity for UV-A and UV-B in the respective wavelength ranges of 315 nm – 400 nm and 280 nm – 315 nm, and zero outside these ranges. Figure 1.1 shows the wavelength dependence for three action spectra with relevance to human health: (1) erythema (McKinlay and Diffey, 1987), (2) pre-vitamin D₃ production in human skin (Holick et al., 2006, after MacLaughlin et al., 1982), and (3) photocarcinogenesis of non-melanoma skin cancers (CIE, 2006). The erythema action spectrum has been accepted for the calculation of the instantaneous UV index (defined as the UV_{ery} irradiance multiplied by 40 (ICNIRP, 1995; WMO, 1997)), and the time-integrated standard erythemal dose ($SED = 100 \text{ J m}^{-2}$ (CIE, 1998)). In practice, use of this CIE spectrum emphasizes the ozone-sensitive region of 295 nm – 320 nm, peaking near 305 nm with minor contributions from longer wavelengths (Madronich et al., 1998; Micheletti et al., 2003). The other two functions are somewhat similar, in that they maximize at around 305 nm wavelength, and decrease by several orders of magnitude by 330 nm.

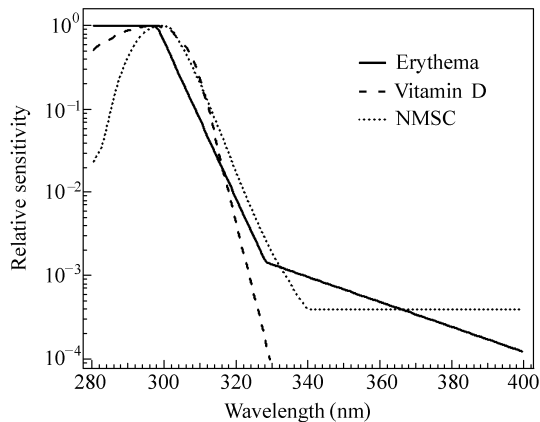


Figure 1.1 Spectral functions for erythema: solid line (McKinlay and Diffey, 1987); synthesis of pre-vitamin D₃: dashed line (MacLaughlin et al., 1982; Holick et al., 2006); and non-melanoma carcinogenesis: dotted line (CIE, 2006)

Compilation of a global UV climatology is computationally intensive, requiring the calculation of $E(\lambda)$ at all relevant wavelengths, at each geographical location, and over diurnal cycles for each day of each year. To reduce computational time, we used the TUV model (Madronich and Flocke, 1997) to pre-tabulate values of weighted UV irradiances as a function of SZA (0° to 96° in 1° steps), ozone column (43 DU – 643 DU in steps of 10 DU), and surface elevation (0, 3, and 8 km above sea level), for cloud-free and aerosol-free conditions. The omission of UV absorption by aerosols can lead to overestimates of irradiance for polluted locations; this limitation will be discussed in more detail later. $E(\lambda)$ at earth's surface was computed at 1 nm steps from 280 nm – 400 nm. The spectral irradiance

incident at the top of the atmosphere was taken from the Atlas3/SUSIM measurements (D. Prinz, pers. comm., 1998). Vertical profiles (appropriate for mid-latitude, annual average conditions) for air density, temperature, and ozone were taken from the U.S. Standard Atmosphere (USSA, 1976) with, however, the ozone profile re-scaled to the actual ozone column (see below). The propagation of solar radiation through the atmosphere was computed with a 4-stream discrete ordinates method (Stamnes et al., 1988), with pseudo-spherical correction for improved accuracy at low sun conditions (Petropavlovskikh, 1995). A Lambertian surface albedo of 5% was assumed at all wavelengths.

The atmospheric ozone column and cloud reflectivity at 380 nm (R) were taken from the TOMS data from three satellites: (1) Nimbus-7, Level 3/Version 8 (McPeters et al., 1996), Nov. 1, 1978 to Dec. 31, 1992; (2) Meteor-3, Level 3/Version 8 (Herman et al., 1996b), Aug. 22, 1991 to Dec. 11, 1994; and (3) Earth Probe, Level 3/Version 8 (McPeters et al., 1998), July 7, 1996 to June 30, 2000. The geographical resolution of the measurements was 1.25° longitude by 1.00° latitude. For each grid point, only one satellite overpass per day occurred (*ca.* local noon). We therefore assumed constant ozone and reflectivity values for the entire day. Local values of the ozone column, SZA and surface elevation were used to compute the clear-sky irradiances at 30-minute intervals over half days by interpolation of the pre-tabulated values. Assuming symmetry about local noon, these data were integrated over 24 hours to obtain the daily UV-A, UV-B, and erythemal doses. A correction for variations in the earth-sun distance was applied as a function of date. A reduction factor F for cloud cover, identical to that used by Eck et al. (1995), was then applied:

$$1/F = \begin{cases} 1 - (R - 0.05)/0.9, & R \leq 50\% \\ 1 - R, & R > 50\% \end{cases}$$

For cloud-free and aerosol-free conditions, total reflectivity at 380 nm is dominated by Rayleigh scattering and surface reflections, the latter being rather small at UV wavelengths unless snow or ice is present. The TOMS algorithm attributes excess reflectivity to clouds or scattering aerosols, without distinguishing between the two. When high surface albedo is encountered (e.g., snow or ice), this method erroneously interprets the high surface reflectivity as cloud cover, thus artificially reducing surface UV irradiance. Polar regions are therefore excluded from our analysis. For non-polar regions, including mountainous regions, we did not attempt to correct for snow cover. The calculated UV doses for such areas should therefore be considered as lower limits.

The calculation of UV doses should in principle be carried out for each location and each day over the satellite record (*ca.* 1979 – 2000). However, gaps in the satellite record exist, so that for some days and/or locations, no doses could be computed. These missing days require some consideration to avoid biases in any

long term averages and trends. For each location, monthly averaged doses were calculated for each of the 247 months in the combined dataset, but were considered valid only if at least half of the days in that month had data. No attempt was made to discriminate between the months in which data gaps typically occurred during the early part of the month and when they typically occurred during the latter part of the month. In some cases, measurements for the same location and days were available from two different satellites; in such cases, monthly means for each satellite were computed, then averaged together to obtain a single mean for that month.

Climatological monthly values were computed for each location by averaging all valid values for that month over multiple years (e.g., climatological January is the mean of all valid January values over 1979 – 2000, etc.). For most of this chapter, we consider averages over the full 22 years (1979 – 2000), but for some of the discussion below, we also considered the time periods 1979 – 1989 and 1990 – 2000 separately. Climatological annual values were computed as the mean of all valid climatological monthly values, specifically (mean of all Jans. + mean of all Febs. + ... + mean of all Decs.)/12.

The second period (1990 – 2000) is missing some data (all of 1995, Jan – Jun 1996, Jul – Dec 2000). We tested the effects of these missing data on the calculated changes by temporarily removing the analogous months from the 1979 – 1989 record and comparing the resulting climatology to that of the complete 1979 – 1989 period. Differences of $< \pm 0.2\%$ were obtained. This is on the order of $\sim 1/10$ of the clear sky changes between the two periods 1979 – 1989 and 1990 – 2000, and on the order of $< 1/10$ of the changes in the “all sky” values between these two periods.

For a comparison with the satellite-derived estimates, we used measurements of UV irradiances by ground-based spectroradiometers, obtained from the World Ozone and UV Data Center archive (WOUDC; data downloaded June 2002). Measured UV_{ery} doses are reported as daily integrals of spectral observations integrated over wavelength with the McKinlay and Diffey (1987) erythemal action spectrum weighting. The archives include 22 non-polar stations; 10 in Canada (Meteorological Service of Canada, MSC); 4 in Japan (Japan Meteorological Agency, JMA); 2 in the Taiwan region (“Central Weather Bureau of Taiwan, CWBT”), and 1 each in Obninsk, Russia (Institute of Experimental Meteorology-Scientific Production Association (IEM-SPA)), Poprad-Ganovce, Slovakia (Slovak HydroMeteorological Institute (SHMI)); Mauna Loa, HI (MSC); San Diego, CA; Ushuaia, Argentina; and Palmer Station, Antarctica (all US National Science Foundation (NSF) sites). The NSF sites operated double monochromators (Biospherical Instruments, Inc), while all other sites operated Brewer single monochromators. Our satellite-based irradiance values for station locations were derived for the locations and altitudes of the ground-based stations.

1.3 Results

1.3.1 Satellite-Derived UV Climatologies

The geographical distributions of daily UV radiation doses at earth's surface, averaged over the entire time period of (Nov. 1, 1978 – June 30, 2000) are shown in Figs. 1.2 – 1.6. The upper panel in each figure shows values calculated by considering the effects of both ozone and clouds, as estimated from TOMS data, and are thus assessed to be nearest to the actual values experienced over this time period. The lower panels show climatological distributions estimated for hypothetical cloud-free skies (i.e., estimated from the ozone distributions without correcting for the presence of clouds).

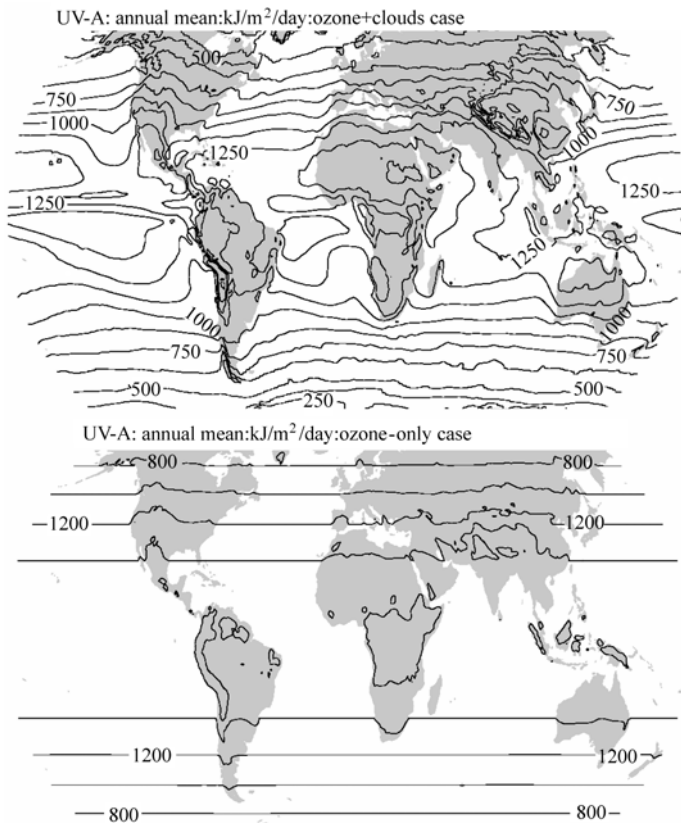


Figure 1.2 Climatological daily doses of UV-A at earth's surface, derived from satellite (TOMS) observations of the atmospheric ozone column and cloud reflectivity at 380 nm and averaged annually over Nov 1, 1978 – June 30, 2000, with (upper) and without (lower) correcting for the presence of clouds

1 A Climatology of UV Radiation, 1979 – 2000, 65S – 65N

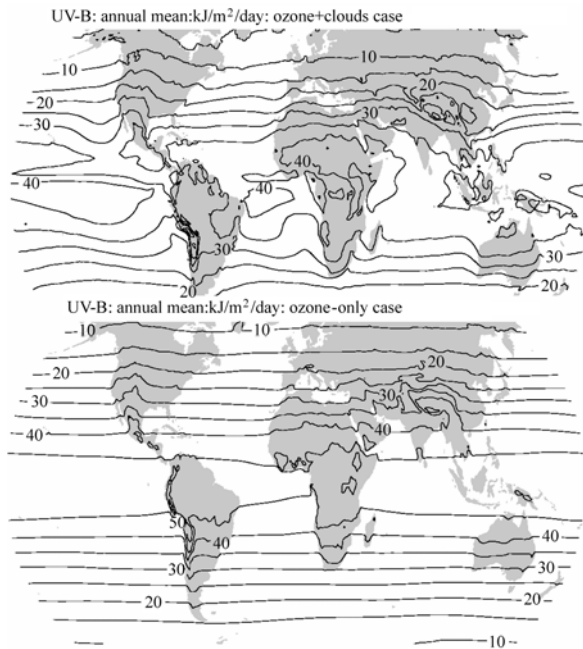


Figure 1.3 Climatological daily doses of UV-B at earth's surface, as Fig. 1.2

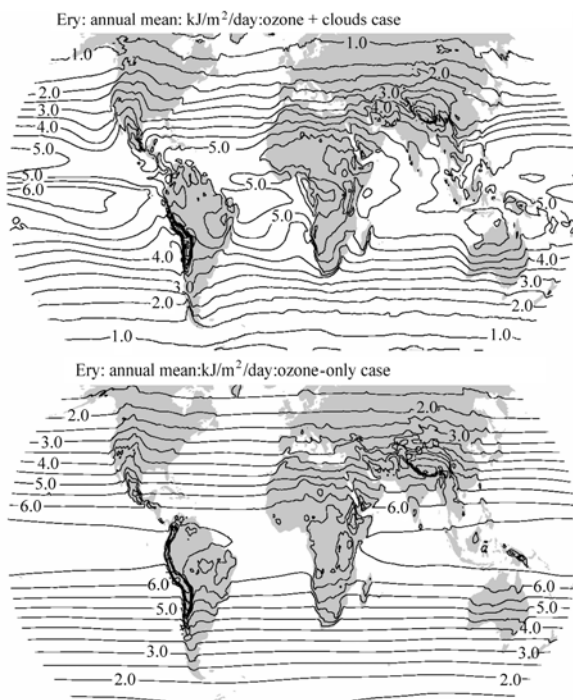


Figure 1.4 Climatological daily doses of erythemal UV at earth's surface, as Fig. 1.2

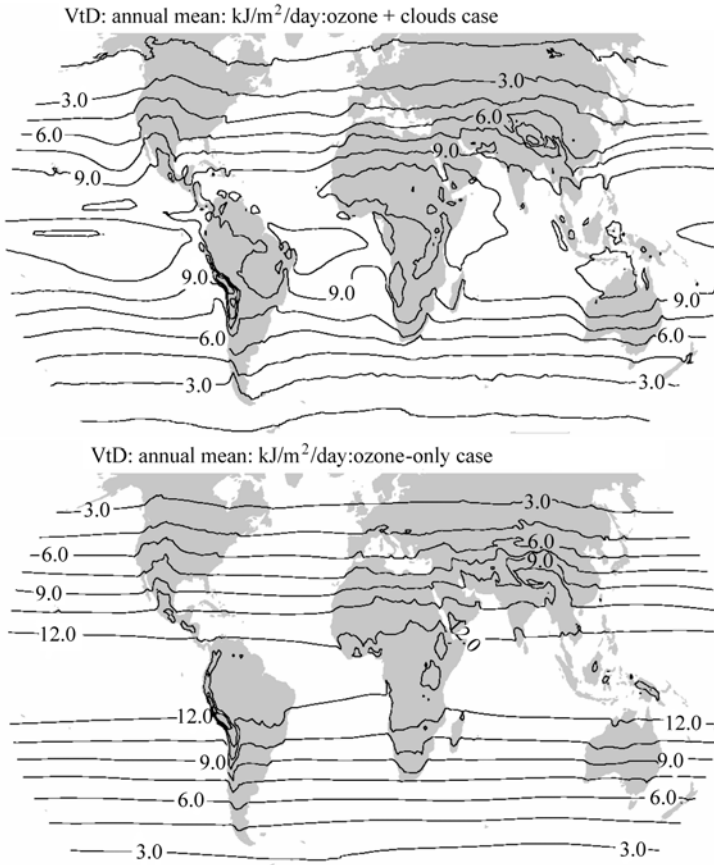


Figure 1.5 Climatological daily doses of UV weighted for pre-vitamin D₃ synthesis at earth's surface, as Fig. 1.2

The zonally homogeneous distribution of UV-A calculated for cloud-free conditions shows almost exclusive dependence on solar position, with only small variations due to surface topography. Ozone column variations induce additional zonal variations in the distributions of cloud-free UV-B and UV weighted for either erythema or other biological response functions. However, the strongest longitudinal variations in the surface UV dose rate distributions are caused by climatological cloud distributions.

As expected, the highest doses are generally seen in the tropics, up to ca. $6 \text{ kJ m}^{-2} \text{ day}^{-1}$ (60 SED day^{-1}) for erythemal UV in the eastern Pacific and eastern Africa, but with substantial cloud-related reductions over western South America, parts of West Africa, and just north of the equator in the eastern and central Pacific. Middle latitudes of both hemispheres show a general pole-ward decrease from about 5 to $1 \text{ kJ m}^{-2} \text{ day}^{-1}$, with some regional highs associated with higher elevations, smaller ozone columns, and infrequent cloudiness (e.g., the Andes

1 A Climatology of UV Radiation, 1979 – 2000, 65S – 65N

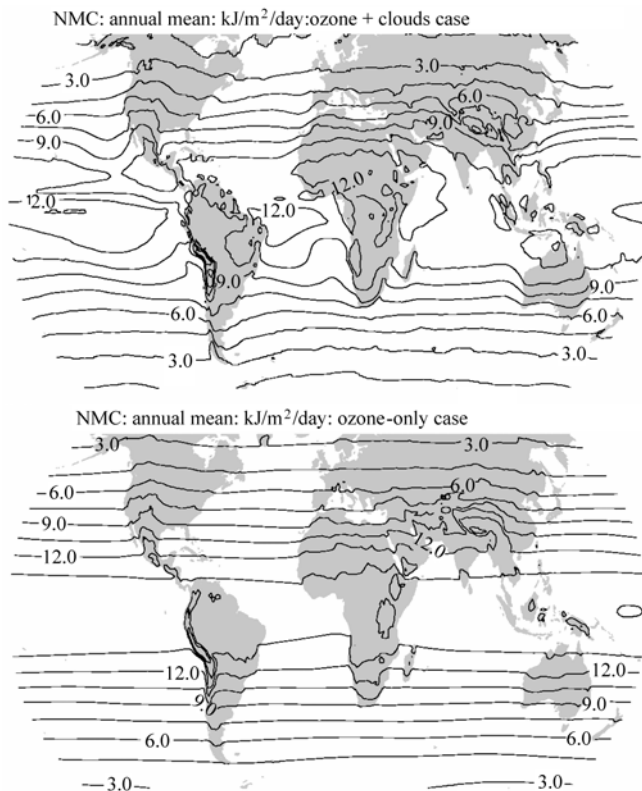


Figure 1.6 Climatological daily doses of UV weighted for non-melanoma carcinogenesis at earth's surface, as Fig. 1.2

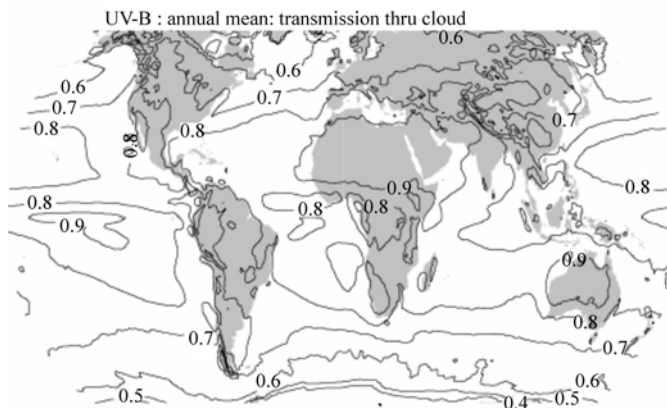


Figure 1.7 Climatological annual mean cloud-related UV reduction factors for daily doses of UV-A derived from satellite (TOMS) observations of the atmospheric ozone column and cloud reflectivity at 380 nm for Nov 1, 1978 – June 30, 2000. Cloud-related UV reduction factors for the other UV functions discussed in this chapter are similar

Mountains, the Tibetan Plateau, central Mexico, and the southwestern U.S.). Lower values for those latitudes are noted for East Asia and the coastal eastern Pacific, associated with more frequent cloud cover. Figure 1.7 shows the cloud-related UV reduction factor, calculated as the ratio of the cloud-corrected climatological daily UV dose (upper panels of Figs. 1.2 – 1.6) to the climatological daily dose before cloud-correction (lower panels of Figs. 1.2 – 1.6).

The seasonal variations of the 22-year UV dose climatologies are shown in Figs. 1.8 – 1.11. (The seasonal variability of UV weighted for non-melanoma carcinogenesis is similar in magnitude and distribution to that of UV weighted for pre-vitamin D3 synthesis, so it is not shown.) The latitudinal distributions are generally consistent with the annual variation of the subsolar point in the tropics, giving strong seasonal variations at temperate latitudes (out of phase by six months between the two hemispheres).

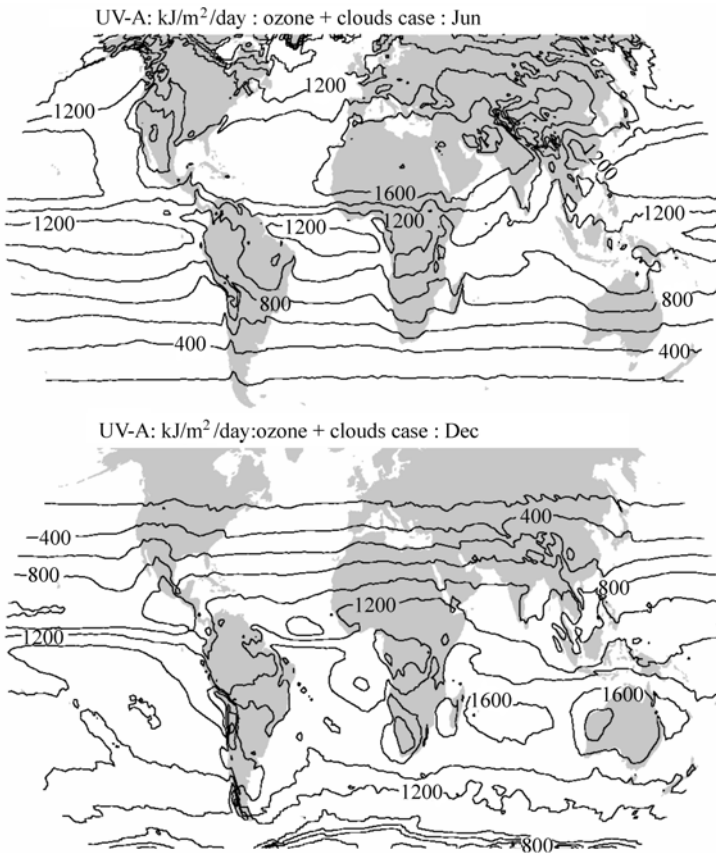


Figure 1.8 Seasonal variability of daily doses of UV-A. The figure shows the daily doses averaged over the period Dec. 1, 1978 – June 30, 2000 for the months of June (upper) and December (lower)

1 A Climatology of UV Radiation, 1979 – 2000, 65S – 65N

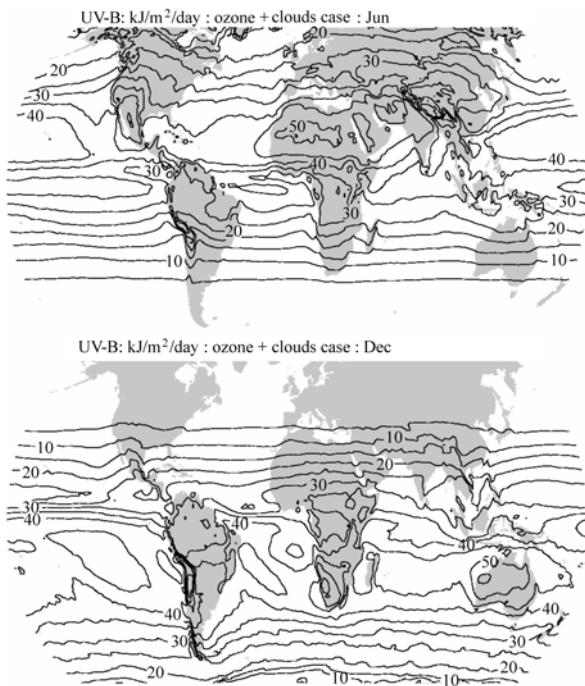


Figure 1.9 Seasonal variability of daily doses of UV-B, as Fig. 1.8

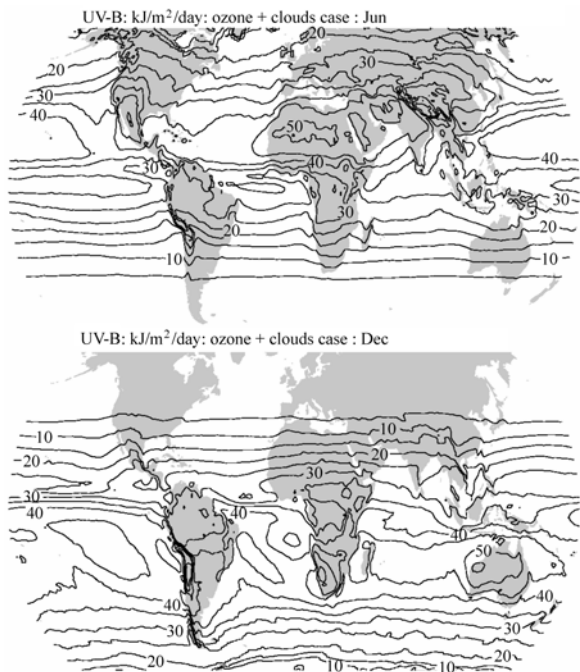


Figure 1.10 Seasonal variability of daily doses of erythemal UV, as Fig. 1.8

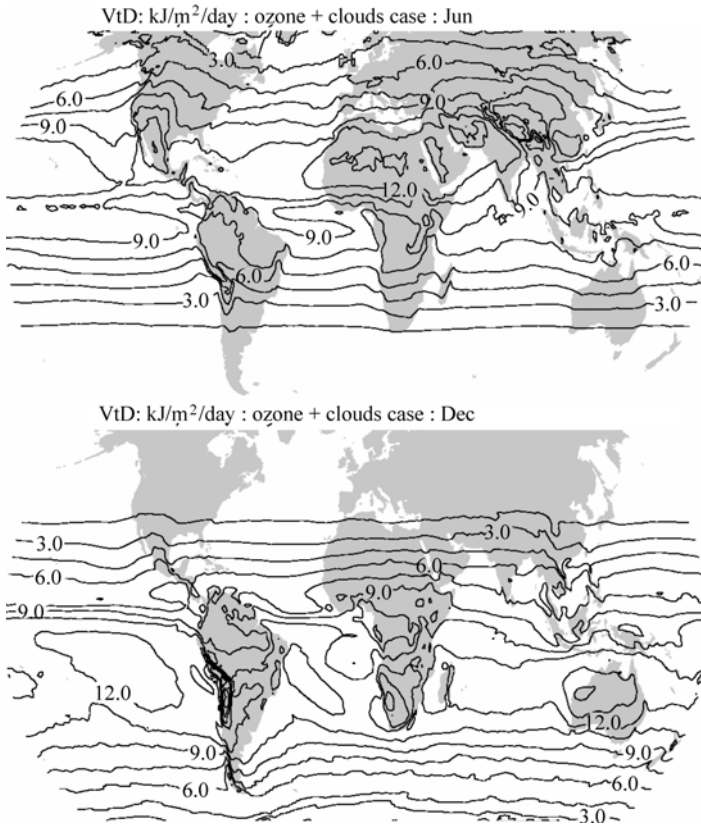


Figure 1.11 Seasonal variability of daily doses of UV weighted for pre-vitamin D_3 synthesis, as Fig. 1.8

Detailed analysis of temporal trends is beyond the scope of this work, but some indications may be obtained by comparing the climatological values averaged over 1990–2000 with those averaged over 1979–1989. Figure 1.12 shows the changes in erythemal doses between these two 11-year periods. The total dose rate changes combine the effects of changes in the ozone column (Fig. 1.12, top panel) and changes in cloudiness (Fig. 1.12, center panel). The upper panel clearly shows the increase in surface UV resulting from stratospheric ozone reductions, not only in the Antarctic region, but also at mid-latitudes. The center panel shows a reduction in cloudiness, maximizing over north-central Europe, possibly as a result of the introduction of cleaner fuel-burning technologies in the west, combined with a contraction of heavy industry in the east. Increases in cloudiness are seen over the Bay of Bengal and over the Humboldt Current off the west coast of South America, possibly owing to the enhanced El Niño conditions prevalent during the 1990s. The apparent reductions in cloudiness around the coasts of

southern Alaska and Hudson Bay may partly be artifacts related to decadal-scale changes in snow and ice cover. The lower panel shows the net change in the annual mean global distribution of erythemal UV dose rates. Significant changes are seen to have occurred, with annual mean dose rate increases of 8% or more in some regions, including north-central Europe, the eastern seaboard of the US, Siberia, and the Antarctic Ocean. Other regions experienced annual mean dose rate reductions of up to 6%.

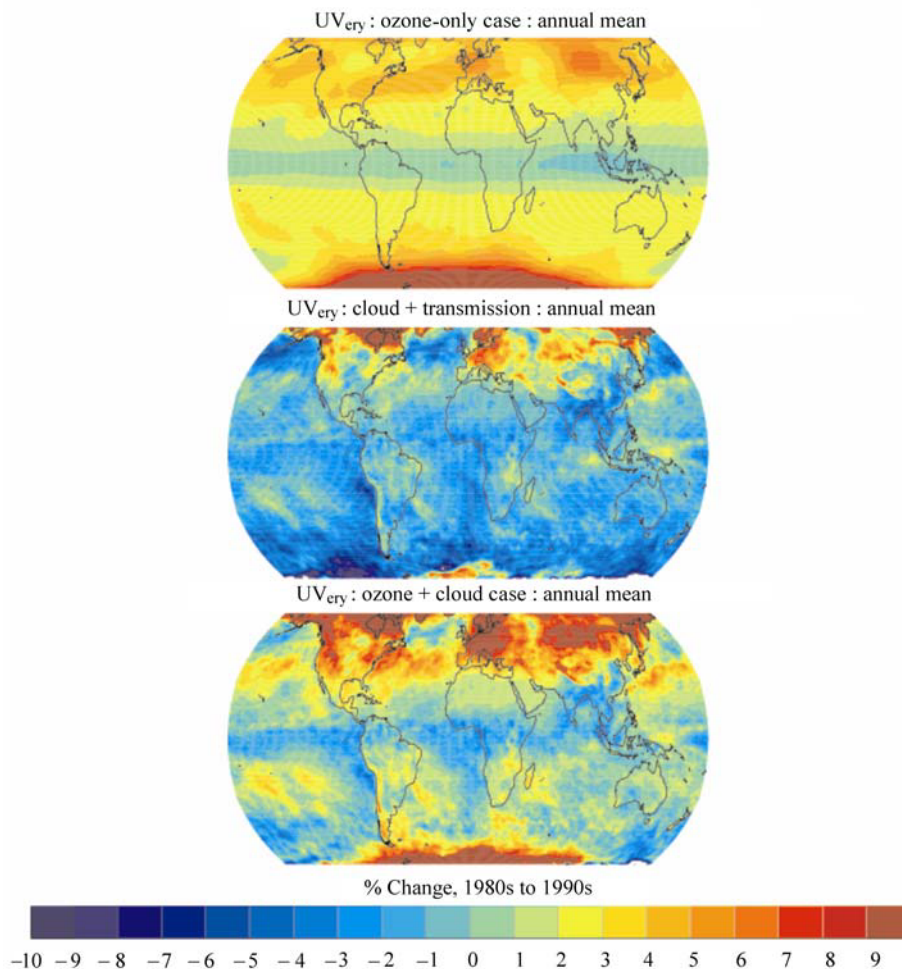


Figure 1.12 Changes in average daily doses of erythemal UV between the periods of 1979 – 1989 and 1990 – 2000. Change in values calculated from the TOMS ozone data only (upper); change in cloud reduction factor (center); change in annual mean net daily erythemal UV dose (lower)

1.3.2 Comparison with Ground-Based Measurements

Comparisons with ground-based measurements are shown in Fig. 1.13 for annual averages of the daily UV_{ery} dose. Temporal overlap between the satellite observations and the ground-based observations is only available at some stations (see Table 1.1), and then only for a few years. The satellite-derived estimates show a long-term trend due to stratospheric ozone depletion, as has been reported previously (Herman et al., 1996a), whether or not cloud cover is considered. Note that the satellite-derived values apply to an extended region of typically 10^4 km^2 , while the ground-based observations pertain to a single, often urban, location. Figure 1.13 shows that the satellite-derived annual averages tend to overestimate measurements by averages of 5% for remote northern locations, 11% for Canadian cities, and 30% for polluted mid-latitude urban regions (San Diego and cities in Japan and cities in the Taiwan region). Herman et al. (1999) found similar differences for the measurements at Toronto, showing also that these were not seasonally dependent, except for snow-covered periods. These discrepancies remain under investigation and may stem from both measurements and satellite-derived values. Because of the imperfect cosine response of the entrance optics, Brewer instruments may underestimate true irradiances by 2% – 7% according to Bais et al. (1998), or by $6\% \pm 2\%$ according to Herman et al. (1999). Network for the

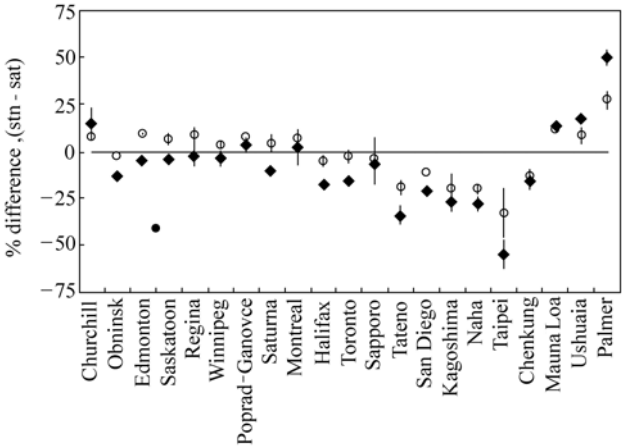


Figure 1.13 Differences between ground-based and satellite-derived annual mean daily erythemal UV doses. Points show the mean of differences for all years where both ground-based and satellite-derived values are available. Lines show the standard deviations at each station. Filled diamonds = satellite-derived UV values including adjustment for the presence of clouds, and mean ground-based values; open circles = satellite-derived UV values without cloud adjustment and maximum ground-based values. Stations are listed in order of decreasing latitude. See Table 1.1 for station details

Table 1.1 Details of ground-based Brewer spectrophotometer stations referenced in Fig. 1.13

Station	Agency*	Station I.D.	Latitude (°)	Longitude (°)	Altitude (m)
Churchill	MSC	77	58.8	–94.1	35
Obninsk	IEM-SPA	307	55.1	36.6	0
Edmonton	MSC	21	53.6	–114.1	766
Saskatoon	MSC	241	52.1	–106.7	550
Regina	MSC	338	50.2	–104.7	592
Winnipeg	MSC	320	49.9	–97.2	239
Poprad-Ganovce	SHMI	331	49.0	20.3	706
Saturna	MSC	290	48.8	–123.1	178
Montreal	MSC	319	45.5	–73.8	24
Halifax	MSC	321	44.7	–63.6	31
Toronto	MSC	65	43.8	–79.5	198
Sapporo	JMA	12	43.1	141.3	19
Tateno	JMA	14	36.1	140.1	31
San Diego	NSF	239	32.8	–117.1	0
Kagoshima	JMA	7	31.6	130.6	283
Naha	JMA	190	26.2	127.7	29
Taipei	“CWBT”	95	25.0	121.5	30
Chenkung	“CWBT”	306	23.1	121.4	10
Mauna Loa	MSC	31	19.5	–155.6	3397
Ushuaia	NSF	339	–54.5	–68.2	7
Palmer	NSF	292	–64.5	–64.0	0

* Agency abbreviations: Meteorological Service, Canada (MSC); Institute of Experimental Meteorology-Scientific Production Association (IEM-SPA), Russia; Swedish Meteorological and Hydrological Institute (SHMI); Japan Meteorological Agency (JMA); National Science Foundation (NSF), USA; “Central Weather Bureau of Taiwan (CWBT).” The World Ultraviolet Radiation Data Centre (WUODC), where the data is archived, has a stated goal of annually intercalibrating the instruments.

Detection of Atmospheric Composition Change (NDACC) quality ground based instruments, which have superior cosine responses and include corrections for these errors, also show much lower UV irradiances than satellite derived values in polluted locations, but good agreement in pristine locations (McKenzie et al., 2001). The TOMS-based method does not account for UV-absorbing aerosols, which according to Herman et al. (1999) lead to a systematic overestimate of ca. $8\% \pm 2\%$ at Toronto. Aerosols are likely to be significant at other locations during pollution episodes (e.g., Wenny et al., 1998), or if an area suffers routinely from pollution (e.g., the Southeast Asian sites). Smaller errors (e.g., 5% or less) are associated with several other factors (e.g., instrument calibrations, extraterrestrial irradiances used in the model), but at present there is no basis for estimating the sign of any resulting bias. The strong disagreement at Palmer Station, where we underestimate the irradiance by 50%, illustrates the consequence of using

TOMS-observed reflectivity to infer cloudiness at high-latitude locations. The high reflectivity recorded by the satellite may be due to snow and ice rather than to clouds, thus leading to a significant underestimate of the UV_{ery} reaching the surface.

Using a similar TOMS-based technique, Frederick and Erlick (1995) computed noon-time erythemal irradiances, as well as their trends and interannual variability, for regions of 6° latitude by 10° longitude centered over New Zealand, Malaysia, Sweden and the eastern U.S. Lubin et al. (1998) used monthly mean ozone from TOMS and monthly mean cloud cover data derived from the Earth Radiation Budget Experiment (ERBE) to compute global UV_{ery} distributions for several months during 1988 and 1989. Sabziparvar et al. (1999) presented a global climatology of daily doses for January, April, July, and October, computed from monthly-averaged climatological ozone (TOMS, 1985 – 1989) and cloud data (International Satellite Cloud Climatology Project (ISCCP), 1983 – 1991). Global distributions of UV_{ery} for 1988 (January, March, July, and September) are presented by Herman et al. (1999), who also carried out detailed comparisons to observations obtained with the Toronto Brewer instrument. Our results are generally consistent with these studies, for example, predicting the strong latitudinal gradients as well as most of the regional anomalies. However, detailed values are not directly comparable because of our use of daily rather than monthly ozone and cloud data, and our integration over an extended time period (1978 – 2000).

1.3.3 Discussion of Uncertainties

We recognize a number of limitations in our study that can hopefully be addressed by future work. The parameterization of cloud effects via the 380 nm reflectivity is obviously crude compared to the complexity of real cloudiness, and its failure in the presence of high albedo surfaces has been discussed. Other sources of cloud information exist and show promise in extending the climatology to higher latitudes (e.g., Mayer and Madronich, 1998). Additionally, pollutants present in the lower atmosphere can attenuate surface UV irradiances. Regional-scale absorbing aerosols, probably associated with plumes of biomass burning, have been detected by the TOMS instrument (Krotkov et al., 1998), although quantification remains a challenging area of research. On smaller scales, such as highly polluted urban areas, substantial absorption of UV radiation is possible from smog-generated ozone, SO_2 , NO_2 , and absorbing aerosols (e.g., soot) in the lower atmosphere. These absorbers are not easily detected from satellite platforms, so that a climatology based on direct ground-based UV radiation measurements, if available, is preferable for such locations.

The presence of snow, whether seasonal or year-round, creates another challenge. The misinterpretation of snow cover as cloud in the satellite data leads to

underestimates of ambient UV. This underestimate stems not only from the inappropriate application of the cloud-related UV reduction factor, but also from the use of a surface albedo of 5%, whereas the reflectivity of snow is usually much higher and causes stronger surface-atmosphere radiative coupling. Hence, even our “cloud-free” climatology may be an underestimate for UV dose in snowy regions. If snow cover is interspersed with lower albedo surfaces such as forest, the bias will be reduced, but not eliminated. Another factor is the increase in effective UV dose received just above a snow surface by reflection from that surface. At higher latitudes and low altitudes, persistent widespread snow is likely to be present only during winter when UV irradiance is already low due to large SZAs. In mountainous regions, snow cover may also persist at lower latitudes, and for longer seasons. In each case, the climatologies presented here underestimate the actual ambient UV dose.

The results shown here do not give the short-term variations in erythemal UV, although some of the inter-annual variability may be inferred from Fig. 1.12. Daily data (1979 – 1994 and 1996 – 2000) are available and were used to compute the long-term averages; however, space limitations preclude their presentation here.

1.4 Conclusions

By using satellite ozone and reflectivity measurements as input to a column radiative transfer model, we have derived near-global climatologies of UV radiation at earth’s surface, weighted for UV-A, UV-B, human erythema induction, pre-vitamin D₃ synthesis, and non-melanoma carcinogenesis. These climatologies are potentially of direct utility to epidemiological studies of the effects of UV exposure, especially if geographical gradients are of interest. For example, the induction of non-melanoma skin cancers is thought to be associated with long-term cumulative exposure to UV radiation, while melanoma mutational subtypes are associated with UV radiation exposure at different life stages (e.g., Thomas et al., 2007). The weighted UV distributions described in this chapter are available for free download from the NCAR Community Data Portal (<http://cdp.ucar.edu>). To find the datasets, navigate the “browse” menu through the directory structure: ACD > ACD Models > TUV > Erythemal UV. A technical note (Lee-Taylor and Madronich, 2007) that includes color versions of the figures in this chapter is also available.

Acknowledgements

This work was supported by the Department of Energy through grants 03-00ER62587.001 and DE-A105-94ER61879 to the National Center for Atmospheric

Research. The National Center for Atmospheric Research is sponsored by the National Science Foundation. Ground-based UV data was obtained from the archive of the World Ozone and Ultraviolet Radiation Data Center (<http://www.woudc.org>).

References

- Bais A, Kazadzis S, Balis D, Zerefos C, and Blumthaler M (1998) Correcting global solar ultraviolet spectra recorded by a Brewer spectroradiometer for its angular response error, *Appl. Optics*, 37, 6339 – 6344
- CIE (Commission Internationale de l’Eclairage) (1998) Erythema Reference Action Spectrum and Standard Erythema Dose, CIE S 007/E-1998, Vienna
- CIE (2006) Photocarcinogenesis Action Spectrum (Non-Melanoma Skin Cancers), CIE S 019/E:2006, Vienna
- Eck TF, Bhartia PK, and Kerr JB (1995) Satellite estimation of spectral UVB irradiance using TOMS derived total ozone and UV reflectivity, *Geophys. Res. Lett.*, 22, 611 – 614
- Frederick JE and Lubin D (1988) The budget of biologically active ultraviolet radiation in the Earth-atmosphere system, *J. Geophys. Res.*, 93, 3825 – 3832
- Frederick JE and Erlick C (1995) Trends and interannual variations in erythemal sunlight, 1978 – 1993, *Photochem. Photobiol.*, 62, 476 – 484
- Herman JR, Bhartia PK, Kiemke J, Ahmad Z, and Larko D (1996a) UV-B increases (1979 – 1992) from decreases in total ozone, *Geophys. Res. Lett.*, 23, 2117 – 2120
- Herman JR, Bhartia PK, Krueger AJ, McPeters RD, Wellemeyer CG, Seftor CJ, Jaross G, Schlesinger BM, Torres O, Labow G, Byerly W, Taylor SL, Swissler T, Cebula RP, and Gu XY (1996b) Meteor-3 Total Ozone Mapping Spectrometer (TOMS) Data Products User’s Guide, NASA Ref. Pub. 1393, Goddard Space Flight Center, Greenbelt, MD
- Herman JR, Krotkov N, Calarier E, Larko D, and Labow G (1999) Distribution of UV radiation at the earth’s surface from TOMS-measured UV-backscattered radiances, *J. Geophys. Res.*, 104, 12059 – 12076
- Herman JR, Piacentini RD, Ziemke J, Celarier E, and Larko D (2000) Interannual variability of ozone and UV-B exposure, *J. Geophys. Res.*, 105, 29189 – 29193
- Holick M (Chair), Bouillon R, Eisman J, Garabedian M, Kleinschmidt J, Suda T, Terenetskaya I, and Webb A (2006) Action Spectrum for the Production of Pre-vitamin D₃ in Human Skin, CIE Technical Report TC 6-54, Vienna
- ICNIRP (International Commission on Non-Ionizing Radiation Protection), Global Solar UV-Index, 1995-1
- Krotkov NA, Bhartia PK, Herman JR, Fioletov V, and Kerr J (1998) Satellite estimation of spectral surface UV in the presence of tropospheric aerosols. 1 Cloud-free case, *J. Geophys. Res.*, 103, 8779 – 8793
- Lee-Taylor J, and Madronich S (2007) Climatology of UV-A, UV-B, and Erythemal Radiation at the Earth’s Surface, 1979 – 2000, NCAR Technical Note TN-474+STR, Boulder, CO

- Lubin D, Jensen EH, and Gies HP (1998) Global surface ultraviolet radiation climatology from TOMS and ERBE data, *J. Geophys. Res.*, 103, 26061 – 26091
- MacLaughlin JA, Anderson RR, and Holick MF (1982) Spectral character of sunlight modulates photosynthesis of pre-vitamin D₃ and its photoisomers in human skin. *Science* 216 (4549): 1001 – 1003
- Madronich S (1992) Implications of recent total atmospheric ozone measurements for biologically active ultraviolet radiation reaching the earth's surface, *Geophys. Res. Lett.*, 19, 37 – 40
- Madronich S, and Flocke S (1997) Theoretical estimation of biologically effective UV radiation at the earth's surface, in *Solar Ultraviolet Radiation-Modeling, Measurements and Effects* (Zerefos, C., ed.). NATO ASI Series Vol. I52, Springer-Verlag, Berlin
- Madronich S, McKenzie RE, Björn LO, and Caldwell MM (1998) Changes in biologically active ultraviolet radiation reaching the earth's surface, *J. Photochem. Photobiol. B: Biology*, 46, 5 – 19
- Mayer B and Madronich S (1998) Calculation of ultraviolet radiation quantities using TOMS ozone and ISCCP cloud data, *Eos Trans.*, 79, F170
- McKenzie RL, Seckmeyer G, Bais A, and Madronich S (2001) Satellite retrievals of erythemal UV dose compared with ground-based measurements at Northern and Southern Latitudes, *J. Geophys. Res.*, 206, 24051 – 24062
- McKinlay AF and Diffey BL (1987) A reference action spectrum for ultraviolet induced erythema in human skin. In: Passchier W.R. and Bosnjakovic, B.F.M. (eds.) *Human Exposure to Ultraviolet Radiation: Risks and Regulations*. Elsevier, Amsterdam
- McPeters RD, et al. (1996) *Nimbus-7 Total Ozone Mapping Spectrometer (TOMS) Data Products User's Guide*, NASA Reference Publication 1384, National Aeronautics and Space Administration, Washington, D.C.
- McPeters RD, et al. (1998) *Earth Probe Total Ozone Mapping Spectrometer (TOMS) Data Products User's Guide*, NASA Tech. Pub. 1998-206895, Goddard Space Flight Center, Greenbelt, MD
- Micheletti MI, Piacentini RD, and Madronich S (2003) Sensitivity of biologically active UV radiation to stratospheric ozone changes: effects of action spectrum shape, *Photochem. Photobiol.*, 78, 456 – 461
- Petropavlovskikh I (1995) Evaluation of photodissociation coefficient calculations for use in atmospheric chemical models, Ph. D. Thesis, U. of Brussels and NCAR/CT-159, Boulder
- Sabziparvar AA, Shine KP, and Forster PM de F (1999) A model-derived global climatology of ultraviolet radiation at the earth's surface, *Photochem. Photobiol.*, 69, 193 – 202
- Stamnes K, Tsay S, Wiscombe S, and Jayaweera K (1988) A numerically stable algorithm for discrete-ordinate-method radiative transfer in multiple scattering and emitting layered media, *Appl. Opt.*, 27, 2502 – 2509
- Thomas NE, Edmiston SN, Alexander A, Millikan RC, Groben P, Hao H, Tolbert D, Berwick M, Busam K, Begg CB, Mattingly D, Ollila DW, Tse CK, Hummer A, Lee-Taylor J, and Conway K (2007) Number of Nevi and Early Life Ambient UV Exposure Are Associated with BRAF-Mutant Melanoma, *Cancer Epidemiology Biomarkers and Prevention*, 16(5), 991 – 997

UV Radiation in Global Climate Change: Measurements, Modeling and Effects on Ecosystems

- UNEP (United Nations Environment Programme), Environmental Effects of Ozone Depletion and Its Interactions with Climate Change: 2006 Assessment (Leun van der, Bornman JC, J, and X. Tang, eds.) United Nations Environment Programme, Nairobi, 2006
- USSA (US Standard Atmosphere) (1976) National Oceanic and Atmospheric Administration (NOAA), National Aeronautics and Space Administration (NASA), United States Air Force, Washington DC
- Wenny BN, Schafer JS, DeLuisi JJ, Saxena VK, Barnard WF, Petropavlovskikh IV, and Vergamini AJ (1998) A study of regional aerosol radiative properties and effects on ultraviolet-B radiation, *J. Geophys. Res.*, 103, 17083 – 17097
- WMO (World Meteorological Organization) (1997) Report of the WMO-WHO Meeting of Experts on Standardization of UV Indices and their Dissemination to the Public, WMO/GAW Report No. 127, Geneva
- WOUDC (World Ozone and UV Data Center) (2002) <http://www.woudc.org/>